
White Rose Research Online

eprints@whiterose.ac.uk
https://eprints.whiterose.ac.uk
Universities of Leeds, Sheffield and York

Deposited via The University of York.

White Rose Research Online URL for this paper:
https://eprints.whiterose.ac.uk/id/eprint/240398/

Version: Accepted Version

Article:
O'GRADY, KEVIN DERMOT, Patel, Vijay, Jones, Iestyn et al. (2026) Magnetic Hyperthermia Based on Hysteresis Heating Alone. IEEE Transactions on Magnetics. ISSN: 1941-0069

https://doi.org/10.1109/TMAG.2026.3686614

Reuse
This article is distributed under the terms of the Creative Commons Attribution (CC BY) licence. This licence allows you to distribute, remix, tweak, and build upon the work, even commercially, as long as you credit the authors for the original work. More information and the full terms of the licence here: https://creativecommons.org/licenses/

Takedown
If you consider content in White Rose Research Online to be in breach of UK law, please notify us by emailing eprints@whiterose.ac.uk including the URL of the record and the reason for the withdrawal request.





Magnetic Hyperthermia Based on Hysteresis Heating Alone

Kevin O'Grady[1,2], *Fellow, IEEE*, Vijay Patel[1], Iestyn Jones[1] and Gonzalo Vallejo-Fernandez[2], *Member, IEEE*
[1]Liquids Research Limited, MENTEC, Deiniol Road, Bangor, Gwynedd, UK, mail@liquidsresearch.co.uk
[2]School of Physics Engineering and Technology, University of York, York, YO10 5DD, UK, gonzalo.vallejofernandez@york.ac.uk

In this work we describe a new approach to magnetic hyperthermia based on hysteresis alone. This is achieved by encapsulating magnetite nanoparticles in polymer spheres to remove dynamic effects which cause unpredictable and uncontrollable heating. This also prevents aggregation of the nanoparticles. To generate significant hysteresis and hence heat, we have used nanoparticles grown by the standard coprecipitation process which are used as seeds and grown to a larger size by the addition of further Fe^{2+} salts in an alkaline solution and heating. We define this as a Controlled Growth Process (CGP). The CGP particles are found to have a much higher saturation magnetisation than particles produced by coprecipitation enhancing their magnetic shape anisotropy. Via magnetic measurements and complementary studies of the heat generated when the polymer spheres are exposed to an ac field, we show that the heat generated is due to hysteresis losses with potentially residual contributions from dynamic effects. At 111 kHz and a maximum applied field of 180 Oe, a specific absorption rate (SAR) value of ∼35 W/g$_{Fe}$ was determined from calorimetry measurements. This value agrees within error with the losses calculated from the hysteresis loop. When the same particles are not encapsulated, significant viscous heating is present.

***Index Terms*—magnetic hyperthermia, hysteresis losses, polymer spheres, iron oxide.**

I. Introduction

MAGNETIC HYPERTHERMIA was proposed as a therapy for the degradation of tissues in the human body as long ago as 1957 [1]. Despite this long history the phenomenon has been slow to achieve widespread application. From the 1990s, significant interest in the subject was generated mainly by work at the Charité Hospital in Berlin under the direction of Andreas Jordan who first published on the subject in 1993 [2] and reported on human trials in 2005 [3]. Several other human trials are now underway, e.g. [4]. There has also been a significant volume of work on the preparation of magnetic nanoparticles for this application [5]. Such particles require regulatory approval for use in vivo which is only currently available for the use of magnetite (Fe_3O_4) and where it occurs, the partial oxidation to maghemite (γ-Fe_2O_3). For a recent review of the state-of-the art the interested reader should refer to Rubia-Rodriguez *et al.* [6].

In 2013 we reported on the physical mechanisms that give rise to heat generation when magnetic nanoparticles dispersed in water are exposed to an ac magnetic field [7]. Via a combination of magnetic and heating measurements together with high resolution particle size analysis, we established that there were three mechanisms that can generate heat. For a given set of experimental conditions, the mechanism by which a particle will generate heat will depend upon their volume. This is shown schematically in figure 1.

Whilst the schematic in figure 1 is shown in terms of the particle diameters, it is the volume that determines the actual behaviour. By way of an example this means that a particle of 8 nm diameter has half the volume of a 10 nm particle.

The smaller particles in the distribution[$D < D_p(0)$] will be superparamagnetic and will not exhibit magnetic hysteresis. $D_p(0)$ is given by,

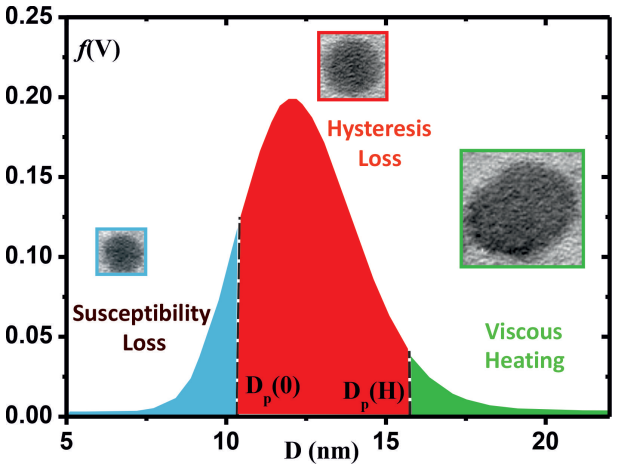


Fig. 1. Schematic diagram showing the different contributions to heat generation from magnetic nanoparticles when cycled at a high frequency magnetic field.

$$D_p(0) = \left[\frac{6k_BTln(tf_0)}{\pi K}\right]^{1/3} \quad (1)$$

where k_B is Boltzmann's constant, T is the temperature of measurement, t is the time of measurement, f_0 is the attempt frequency and K is the anisotropy constant of the particle.

Note that the value of D_p depends on the time of measurement and hence varies with frequency which in this case was 111.5 kHz. Such particles will attempt to follow the field at lower frequencies thereby generating heat via susceptibility loss [7]. Above $D_p(0)$ the particles will be blocked and exhibit normal ferromagnetic behaviour i.e. hysteresis, with a coercivity depending on their volume V according to

$$H_c = H_K \left[1 - \left(\frac{9.1 k_B T}{KV}\right)^{1/2}\right] \quad (2)$$

where the factor 9.1 is the value of $ln(tf_0)$ evaluated at 111.5 kHz and assuming f_0 = 10^9 s^{-1} and H_K is the anisotropy field which, in the case of randomly oriented magnetic nanoparticles, is equal to $0.96K/M_s$ [8], where M_s is the saturation magnetisation of the particles.

Due to the limited field available on our heating apparatus and which will be the case in vivo due to the pain threshold for larger fields [9], the larger particles will not be able to switch. However, as they are in a liquid such particles can rotate to align with the field which will generate viscous heating i.e. stirring. This is an unpredictable and uncontrollable source of heat that will limit the applicability of magnetic hyperthermia in vivo. It should also be noted that if a stable colloidal dispersion is injected into a body, then the different chemical environment will almost certainly destabilise the colloid leading to particle aggregation which may enhance the heating effect due to stirring. We seek to address these issues in this work.

The heating power generated by susceptibility loss is given by [10]

$$P_{AC} = \pi f \chi" H^2 \quad (3)$$

The parameter χ" is the complex part of the ac susceptibility given by

$$\chi" = \frac{2\pi f\tau}{1 + (2\pi f\tau)^{1/2}} \chi_0 \quad (4)$$

where χ_0 is the dc susceptibility and τ is the combined relaxation time due to both Brownian and superparamagnetic relaxation times which are given by

$$\tau_B = \frac{3V_h\eta}{k_B T} \quad (5)$$

$$\tau_N = \frac{1}{f_0} exp\left[\frac{KV\,(1 - H/H_K)^{1/2}}{k_B T}\right] \quad (6)$$

where V_h is the hydrodynamic volume of the particle and η is the viscosity of the solution. In our original work we found that susceptibility loss generated less than 5% of overall heating but it should be noted that our measurements were made in a low field of $<$10 Oe.

The heating power due to hysteresis losses is given by the frequency of the field multiplied by the area of the hysteresis loop. However due to the variation of the loop area with the particle size this must be integrated over the particle volume distribution between $V_p(0)$ and $V_p(H)$ where H represents the maximum applied field and $V_p(H)$ is related to $V_p(0)$ as follows

$$V_p(0) = \left[1 - \frac{HM_s}{0.96K}\right]^2 V_P(H) \quad (7)$$

Hence the power dissipated via hysteresis losses is given by

$$P_{HYS} = 2fM_s \int_{V_p(0)}^{V_p(H)} H_c(V) f(V) dV \quad (8)$$

where $V_p(0)$ and $V_p(H)$ correspond to the critical volume for superparamagnetic behaviour and the maximum particle volume that can be switched under an applied field H, respectively. In practice, there is also a distribution of anisotropy constants that needs to be taken into account in eqn. 8 [11]–[13]. It is not possible to calculate the heating power due to particle rotation as the particles will not be smooth spheres and may form elongated chains due to dipolar interactions and the rms value of the ac field. However, we measured this contribution by dispersing the same particles in a light paraffin oil and a high melting point paraffin wax. This revealed that in our samples 40% of the heat generated came from dynamic effects, i.e. stirring [7].

II. Nanoparticle Dynamics

As shown in equation 5 the Brownian relaxation time (τ_B) for a magnetic sphere varies linearly with volume or the cube of the diameter. This simple relationship is shown in figure 2 for colloids having viscosities of 1 cP and 10 cP. The figure shows that a spherical particle having a diameter of 10 nm would have a relaxation time of 2.3x10^{-4} s. This would lead to such a particle rotating at a frequency of up to 400 kHz. Of course this is an approximate calculation as the volume in equation 5 is the hydrodynamic size which is not known with any certainty. However, for a sphere having a diameter of 1 μm the relaxation time is increased by a factor of 10^6 so such an entity would not be able to rotate at even 1 Hz. Even in water such a particle would in effect be in a solid environment and could not rotate to follow an ac field of any significant frequency.

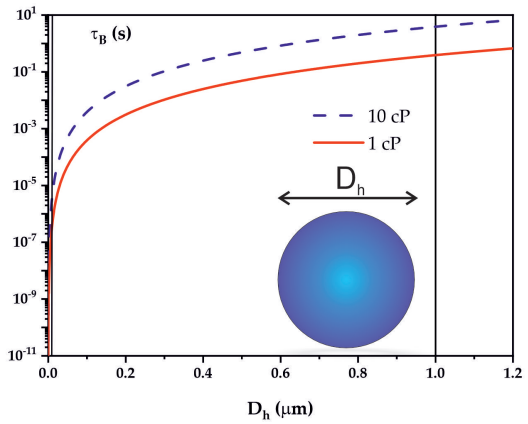


Fig. 2. Brownian relaxation time as a function of hydrodynamic size at 293 K for two difference viscosity values.

In principle this would be the case for 1 μm magnetic particles but such entities would not be single domain particles and would not exhibit significant hysteresis. They would also be strongly aggregated preventing the formation of a uniform dispersion.

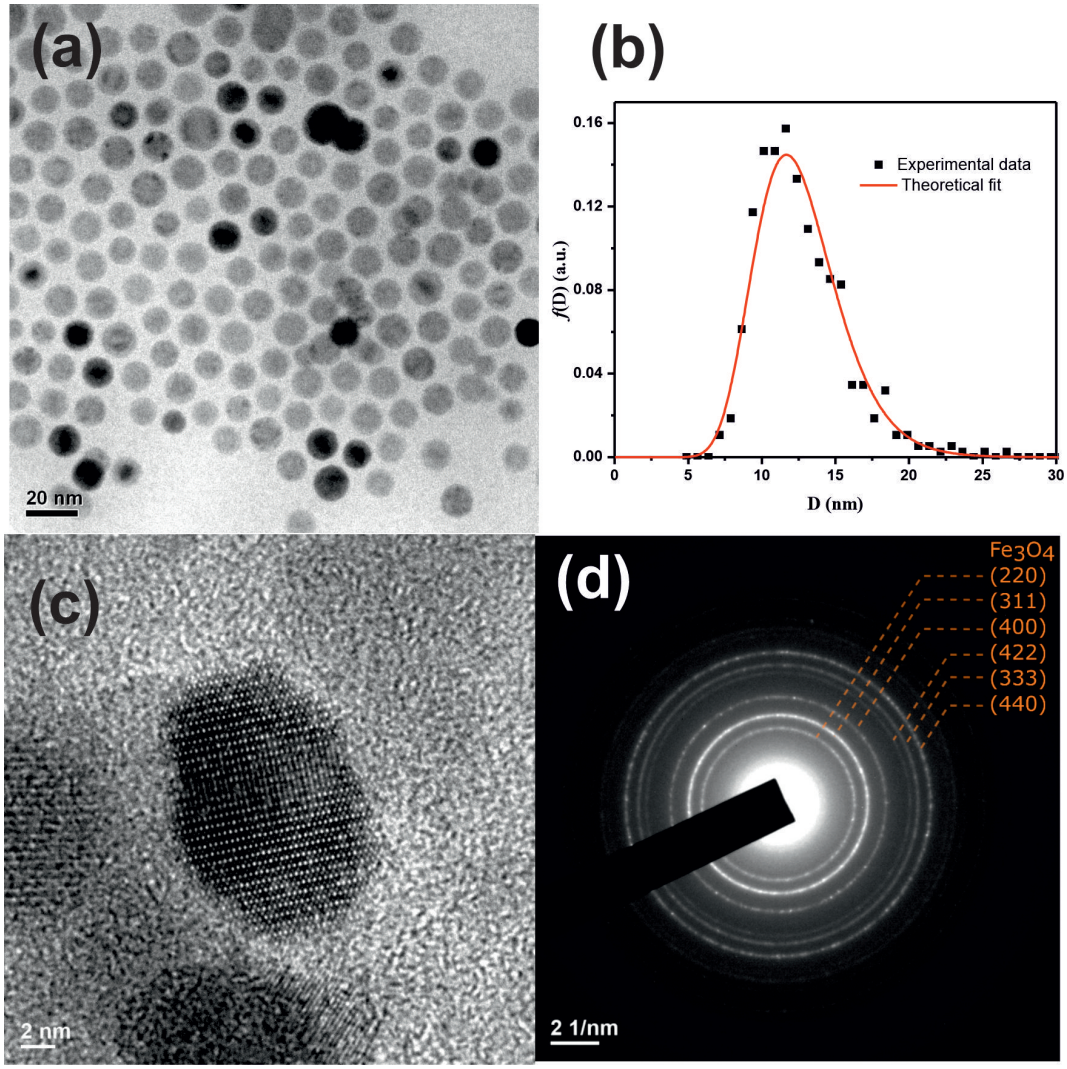


Fig. 3. (a) Bright field TEM image; (b) particle size distribution; (c) High resolution TEM image; (d) Selected area diffraction pattern for the CGP particles.

We have overcome this problem by dispersing nanoparticles in 1 μm polymer spheres. This prevents aggregation in any environment and allows for functionalisation for targeted therapies. The hysteresis has been enhanced by growing the particles to a slightly larger size, 15 nm, than those commonly used as described below.

III. Sample Preparation

The initial stage of the nanoparticle growth was undertaken by the standard coprecipitation process. An Fe^{3+} salt such as $FeCl_3.6H_2O$ (142.6 g) was dissolved in distilled water giving a total volume of 400 ml. A second solution of $FeCl_2.4H_2O$ (111.2 g) was also dissolved giving a total volume 400 ml. The two solutions were combined and stirred. The mixed solution was added to a 10 M NaOH solution via a peristaltic pump at a rate of 17 ml/minute with rapid stirring producing a black precipitate which was stirred for a further 30 minutes. The resulting magnetite nanoparticles were washed several times in water to remove the remaining salts. The particles had a median diameter of circa 9 nm.

After washing, the particles were added to a 10 M solution of NaOH giving a pH of 12. The slurry was stirred at 500 rpm. To create a growth layer, 65 ml of an $FeCl_2.4H_2O$ solution of 1.0 M was added at 250 ml/minute by peristaltic pump. Due to the slow addition rate no further nucleation occurred. The slurry was stirred for one hour and heated to 100°C with continued stirring for a further hour. The particles were then coated with oleic acid in alkali solution with heating. The resulting particles were then washed with water at least 6 times and once with acetone to remove excess oleic acid. The resulting particles are shown in the TEM image in figure 3(a) and the particle diameter distribution is shown in figure 3(b). We refer to this growth as the Controlled Growth Process (CGP). The CGP process has been patented [14].

The CGP particles are highly crystalline as shown in the high-resolution TEM image at figure 3(c) where the lattice is seen to extend to within a few atom layers of the surface as well as the selected area diffraction pattern shown in figure 3(d). The addition of the growth layer also restores the overall balance of the Fe^{3+}/Fe^{2+} closer to the ideal ratio of 2:1 and the presence of a richer Fe^{2+} surface also aids the

bonding of the oleic acid to the particles so that little primary aggregation is seen in figure 3(a). As a result, the saturation magnetisation of the uncoated particles determined using a vibrating sample magnetometer is between 80 and 85 emu/g compared to the coprecipitated particles which have a value closer to or less than 70 emu/g.

Demonstration polystyrene polymer spheres loaded with CGP particles were prepared using a suspension polymerization method. First, the oleic acid coated CGP particles were dispersed in a monomer mixture of 97% styrene and 3% divinyl benzene using a phosphate ester as a secondary dispersant. An organic peroxide initiator was then incorporated into the dispersion and the resulting ferrofluid was emulsified in water in a ratio of 1:5 using a high shear mixer. The emulsion was then heated to 80°C under N_2 for 16 hours giving the CGP loaded polymer spheres. The % loading of CGP particles was determined to be approximately 40% by measuring the dried polymer spheres using a VSM and comparing the magnetization of dried CGP particles. Figure 4 shows a typical scanning electron microscope image of the resulting spheres.

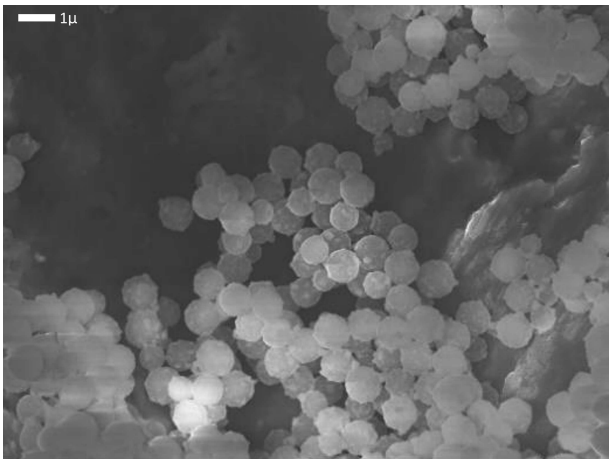


Fig. 4. Scanning electron microscope image of the polymer spheres used in this study

IV. Heating Experiments

Heating experiments were performed using a modified nanoTherics Magnetherm system. It consists of a sample coil enclosure, a function generator and a power amplifier forming a resonant circuit. The system is monitored by an output from the coil to an oscilloscope. The modification consists of a new design of the measurement cell. In a previous work we described a method for the determination of the heating power of magnetic nanoparticle colloids where the improvements to the measurement cell were presented in detail. The method is based upon a comparison between the heating power observed when the colloid is exposed to a radio frequency magnetic field and that which is observed using a resistive electrical heater. This together with the new cell offered the following advantages: (a) it allowed to account for heat losses to the environment; (b) it minimised the effect of convection currents which can result in the temperature measured not being representative of the samples as whole; (c) it ensured the field was uniform to ±10% [15].

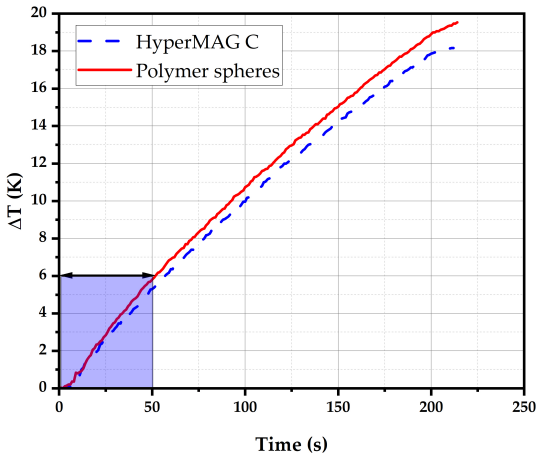


Fig. 5. Initial heating rate for a sample consisting of HyperMAG C particles dispersed in water (blue dashed line) and a sample consisting of the same particles encapsulated in polymer spheres (red solid line). The experiments were performed at 111 kHz with a maximum applied field of 180 Oe. The shaded area corresponds to the initial heating region used for the SAR calculation.

Figure 5 shows an example of the initial heating curves for an aqueous dispersion of the particles and encased in polymer spheres. The samples were measured at 111 kHz and a field amplitude of 180 Oe. Each measurement was repeated three times after the system had cooled down to the same starting temperature. The SAR values for both samples were calculated using

$$SAR = \frac{C\rho}{\phi}\frac{\Delta T}{\Delta t} \tag{9}$$

where C is the specific heat of the colloid, ϕ is the concentration of Fe per ml of solution, ρ is the density of the colloid and $\Delta T/\Delta t$ represent the heating rate which can be calculated from data such as that shown in figure 5. For the calculation, only the first 50 s of the data shown in figure 5 were used. This resulted in heating rates of (0.115±0.003) and (0.127±0.001) K/s for the standard and polymer sphere samples, respectively, where the errors arise from the standard error in the mean after three measurements. While only qualitatively, these errors seem to suggest that the measurements for the polymer spheres are more uniform across different runs.

The non-encapsulated particles were dispersed in deionised water with a specific heat capacity of 4.184 J/gK and a density of 1 g/cm^3. The concentration of Fe in the particles was 10 $\mathrm{mg}_{Fe}/\mathrm{ml}_{solution}$.

For the polymer sphere sample the calculation is a bit more complicated as the concentration of Fe in the sample had to be calculated from the saturation magnetisation of the fluid and the equivalent value for the non-encapsulated sample. The specific heat capacity can be assumed to be similar to that of the regular sample as the polymer has a lower specific heat capacity than the deionised water. From vibrating

sample magnetometer (VSM) measurements, the saturation magnetisation of the polymer sphere sample was 1.58 emu/g and its density 1.02 g/cm^3. Based on this, the concentration of iron in the polymer sphere sample was determined as (15.4±0.2) mg$_{Fe}$/ml$_{solution}$.

The SAR value for the HyperMAG C sample was determined as (48±2) W/g$_{Fe}$. The corresponding rate for the polymer sphere sample was significantly lower (∼27%) with a measured value of (35±1) W/g$_{Fe}$. In the case of the free particles, most of the error comes from the determination of the initial heating rate. However, for the encapsulated particles the more complicated estimation of the concentration of Fe in the sample dominates the uncertainty.

V. Magnetic Measurements

The magnetic properties of the samples were measured using a home built high frequency hysteresis loop tracer. The system has been described in detail previously [16] with a resonant circuit being used to create an alternating current at a series of defined frequencies. The system uses three MnZn ferrite rods to enhance the maximum field. Fields as high as 420 Oe can be applied by passing a current as low as 2.5 A through the primary at all operating frequencies. Careful consideration has been given to the shape of the sample holder so as to minimise the demagnetising field. Overall an aspect ratio of 3:1 was deemed a reasonable compromise which results in a sample volume of ∼7μL. This results in a demagnetising field at saturation of 13.4 Oe and 20.7 Oe for the HyperMAG C and polymer sphere samples, respectively. In practice, the demagnetising field at any point in our hysteresis loop measurements is much smaller as the maximum applied field is smaller than that required to saturate the samples. The sample holders were filled using a Fisherbrand Elite adjustable volume pipette (2-20μL, ±0.1 μL with 0.2 μL increments).

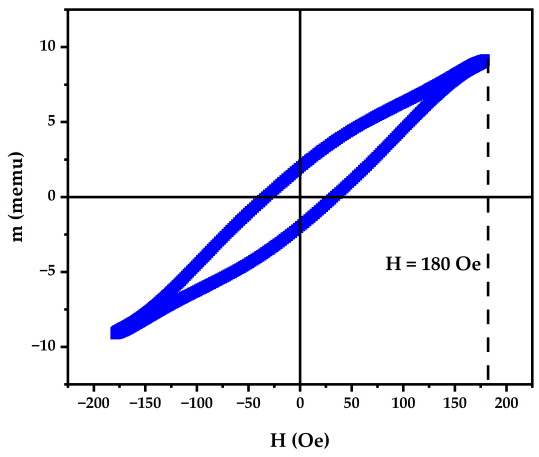


Fig. 6. Hysteresis loop measured at 111 kHz for the sample containing magnetite nanoparticles encapsulated in polymer spheres.

Our heating experiments were performed using a Nanotherics Magnetherm at an operating frequency of 111 kHz and a maximum applied field of 180 Oe. Since many hyperthermia experiments are performed at a frequency of ∼111 kHz, a capacitor bank with an equivalent capacitance of 3.1 nF was used which results in an operating frequency of 111 kHz. Figure 6 shows the hysteresis loop for the polymer spheres sample measured using these conditions. Since the sample was not fully saturated at the maximum applied field of 180 Oe, a calibration factor needed to be applied so that the area under the hysteresis loop could be calculated in units of Joules. This was achieved by fitting a sigmoidal function to one of the branches of the hysteresis loop and extrapolating. Given that 7 μl of fluid were used, a moment of 11.5 memu was expected at saturation. There is likely to be a significant error in the moment of the sample calculated this way which we expect to be of the order of 15%.

By calculating the area under the hysteresis loop and multiplying it by the frequency of operation, the power dissipated can be calculated as 4.26 mW. In order to calculate a SAR value so that it can be compared to the value measured using the Magnetherm system, the amount of Fe in the sample needs to be calculated. Given the volume of the sample and the Fe concentration in the polymer spheres, this results in 0.108 mg. Hence, the power dissipated via hysteresis losses alone calculated from the data shown in Figure 6 is (39±6) W/g$_{Fe}$. Most of the uncertainty comes from the error determining the moment of the sample. This result is in good agreement with the data obtained using the Magnetherm system with both results agreeing within the combined experimental uncertainty.

Similar analysis for the HyperMAG C sample leads to a hysteretic heating of (23±3) W/g$_{Fe}$. This value is significantly lower than that obtained using the Magnetherm system confirming the presence of significant viscous heating due to the particles progressively aligning with the applied field.

VI. Conclusions

We have shown that by encapsulating iron oxide magnetic nanoparticles in polymer spheres the amount of heat generated when cycling the particles in a high frequency magnetic field can be predicted accurately. The heating arises from hysteresis losses alone with undesirable viscous heating being suppressed within error. The results presented in this work can be extended to different frequencies of operation as it allows for the particle size to be tailored depending on the desired frequency. This allows for hysteresis losses to be optimised to a specific application. Hence, this approach opens the possibility for predictive hyperthermia experiments to be performed. Obviously the use of polymer spheres will result in the introduction of micron-scale carriers which might affect biodistribution and tumour penetration. This might lead to slower or less predictable clearance pathways compared to free nanoparticles. The extent of this unknown and highlights the importance of optimising the carrier design to balance the heating performance with effective biological delivery.

As indicated, the results for the polymer spheres show improved run-to-run consistency under identical conditions for a given sample as no magnetic particle aggregation can occur. Reproducibility can be assessed via the magnetic data. In this way it will be possible to inform dose estimation for a desired

therapeutic outcome in any tissue if the heat loss due to blood flow is known or can be calibrated.

VII. Data Availability

The data that support the findings of this study are available upon reasonable request from the authors.

References

[1] R. K. Gilchrist, R. Medal, W. Shorey, R. C. Hanselman, J. C. Parrott, and C. B. Taylor, *Annals Surgery*, vol. 146, no. 4, pp. 596–606, October 1957.

[2] A. Jordan, P. Wust, H. Fählin, W. John, A. Hinz, and R. Felix, *International Journal of Hyperthermia*, vol. 9, no. 1, pp. 51–68, 1993.

[3] M. Johannsen, U. Gneveckow, L. Eckelt, A. Feussner, N. WaldoFner, R. Scholz, S. Deger, P. Wust, S. A. Loening, and A. Jordan, *International Journal of Hyperthermia*, vol. 21, no. 7, pp. 637–647, 2005.

[4] C. Caizer. John Wiley Sons, Ltd, 2021, ch. 18, pp. 430–463.

[5] S. Mishra and M. D. Yadav, "Magnetic nanoparticles: A comprehensive review from synthesis to biomedical frontiers," *Langmuir*, vol. 40, no. 33, pp. 17 239–17 269, 2024, pMID: 39132737. [Online]. Available: https://doi.org/10.1021/acs.langmuir.4c01532

[6] I. Rubia-Rodríguez, A. Santana-Otero, S. Spassov, E. Tombácz, C. Johansson, P. De La Presa, F. J. Teran, M. d. P. Morales, S. Veintemillas-Verdaguer, N. T. K. Thanh, M. O. Besenhard, C. Wilhelm, F. Gazeau, Q. Harmer, E. Mayes, B. B. Manshian, S. J. Soenen, Y. Gu, Millán, E. K. Efthimiadou, J. Gaudet, P. Goodwill, J. Mansfield, U. Steinhoff, J. Wells, F. Wiekhorst, and D. Ortega, "Whither magnetic hyperthermia? a tentative roadmap," *Materials*, vol. 14, no. 4, 2021.

[7] G. Vallejo-Fernandez, O. Whear, A. G. Roca, S. Hussain, J. Timmis, V. Patel, and K. O'Grady, *Journal of Physics D: Applied Physics*, vol. 46, no. 31, p. 312001, jul 2013.

[8] F. E. Luborsky, "Development of elongated particle magnets," *Journal of Applied Physics*, vol. 32, no. 3, pp. S171–S183, 03 1961. [Online]. Available: https://doi.org/10.1063/1.2000392

[9] Q. A. Pankhurst, J. Connolly, S. K. Jones, and J. Dobson, *Journal of Physics D: Applied Physics*, vol. 36, no. 13, p. R167, jun 2003.

[10] R. Rosensweig, "Heating magnetic fluid with alternating magnetic field," *Journal of Magnetism and Magnetic Materials*, vol. 252, pp. 370–374, 2002, proceedings of the 9th International Conference on Magnetic Fluids. [Online]. Available: https://www.sciencedirect.com/science/article/pii/S0304885302007060

[11] G. Vallejo-Fernandez and K. O'Grady, "Effect of the distribution of anisotropy constants on hysteresis losses for magnetic hyperthermia applications," *Applied Physics Letters*, vol. 103, no. 14, p. 142417, 10 2013. [Online]. Available: https://doi.org/10.1063/1.4824649

[12] A. A. McGhie, C. Marquina, K. O'Grady, and G. Vallejo-Fernandez, "Measurement of the distribution of anisotropy constants in magnetic nanoparticles for hyperthermia applications," *Journal of Physics D: Applied Physics*, vol. 50, no. 45, p. 455003, oct 2017. [Online]. Available: https://dx.doi.org/10.1088/1361-6463/aa88ed

[13] D. Clarke, C. Marquina, D. Lloyd, and G. Vallejo-Fernandez, "Effect of the distribution of anisotropy constants on the magnetic properties of iron oxide nanoparticles," *Journal of Magnetism and Magnetic Materials*, vol. 559, p. 169543, 2022. [Online]. Available: https://www.sciencedirect.com/science/article/pii/S0304885322004644

[14] K. O'Grady, "Microparticles for magnetic hyperthermia,," *U.S. Patent US20240041784, UK Patent GB2621146*, 2024.

[15] A. Drayton, J. Zehner, J. Timmis, V. Patel, G. Vallejo-Fernandez, and K. O'Grady, "A comparative measurement technique of nanoparticle heating for magnetic hyperthermia applications," *Journal of Physics D: Applied Physics*, vol. 50, no. 49, p. 495003, nov 2017. [Online]. Available: https://dx.doi.org/10.1088/1361-6463/aa95d8

[16] D. Clarke and G. Vallejo-Fernandez, *Journal of Magnetism and Magnetic Materials*, vol. 552, p. 169249, 2022.